Chemical Physics Letters 756 (2020) 137843

Contents lists available at ScienceDirect

Chemical Physics Letters

journal homepage: www.elsevier.com/locate/cplett

Research paper

Ultrafast Coherent Anti-Stokes Raman spectroscopic studies of nitro/nitrogen rich aryl-tetrazole derivatives

Naga Krishnakanth Katturi[a], Sarang Dev G[a], Nagarjuna Kommu[a], Gopala Krishna Podagatlapalli[b,*], Venugopal Rao Soma[a,*]

[a] Advanced Centre of Research in High Energy Materials (ACRHEM), University of Hyderabad, Hyderabad 500046, Telangana, India
[b] Department of Electronics& Physics, GIS, GITAM deemed to be University, Visakhapatnam 530045, Andhra Pradesh, India

HIGHLIGHTS

- Femtosecond CARS data of nitro-substituted tetrazole-N-(hetero)aryl derivatives reported.
- Femtosecond CARS transients and FFT revealed possible IVR mechanisms.
- The dephasing times were found to be < 200 fs for both the molecules investigated.
- Molecule with superior energetic properties possessed faster relaxation times.

ARTICLE INFO

Keywords:
Femtosecond CARS
Intramolecular vibrational relaxation
Energetic molecules
Dephasing time

ABSTRACT

We report the time and frequency-resolved coherent anti-Stokes Raman spectroscopy (CARS) data of nitro-substituted tetrazole-N-(hetero)aryl derivatives with ~ 50 fs pulses. CARS experiments were performed to comprehend the intramolecular vibrational redistribution (IVR) dynamics through vibrational couplings in Amino (6) and Nitro (8) substituted tetrazoles. The present study elevates the applications of tetrazoles derivatives since their energetic properties are comparable with the secondary explosives RDX/TNT. The Fourier transforms of the CARS transients revealed the possible IVR mechanisms in tetrazole-N-(hetero)aryl derivatives. Further, the average coherent vibrational decay time (T_2) were estimated to be in the range of ~120–200 fs from the CARS transients.

1. Introduction

The invention of ultrafast lasers brought novel possibilities of probing and understanding the ultrafast phenomena such as electronic and vibrational dynamics in the ground/excited state of the molecules [1–4]. Energetic materials (EMs) store enormous energy in the chemical form that can be easily converted to kinetic energy by molecular decomposition and retrieved energy can be used in industrial and military applications [5]. Excited-state dynamics of the energetic materials provide an insight into the molecular decomposition mechanisms for different ignition processes, such as heat, shock and compression waves etc. [5,6]. The compression of the material at a pressure of 30 GPa or above could induce an electronic excitation nearly equal to the lowest singlet excited states of EMs [6,7]. The investigation of the electronic, chemical and structural changes of the excited states of EMs enables us to understand the behaviour of EMs at the molecular level. Consequently, a lot of research has been performed to understand the reaction mechanisms in EMs along with the enhanced safety measures [8–13]. The non-radiative transitions of the excited states of the molecules produce local heating that causes to form hotspots which initiate the chain reactions in EMs [14]. Infrared (IR) photons play a prominent role in the generation of such hotspots [15]. In the microscopic view, the heat or shock front can be regarded as the superposition of vibrations of chemical bonds and the shock waves influence the EMs to undergo a series of energy transfer processes prior to the disruption of these bonds. When an EM interacts with a shock wave, initially, a number of phonons will be generated and later, the low-frequency vibrational modes get excite through phonon-vibron coupling i.e. multi-phonon up-pumping [16,17]. Further, the vibrational energy transfer occurs from one vibrational mode to the other known as intramolecular vibrational redistribution (IVR). During the IVR, distributed energies localized in one or a few chemical bonds dissociate and trigger the

* Corresponding authors.
E-mail addresses: gpodagat@gitam.edu (G.K. Podagatlapalli), soma_venu@uohyd.ac.in (V.R. Soma).

https://doi.org/10.1016/j.cplett.2020.137843
Received 31 March 2020; Received in revised form 30 July 2020; Accepted 31 July 2020
Available online 06 August 2020

ignition [18]. Therefore, IVR directly affects the vibrational energy transfer and the breaking of chemical bonds in EMs. However, the visualization of ultrafast coherent phenomenon such as IVR is tedious since it involves the coupling of several vibrational modes [18]. In this context, excitation and relaxations of vibrational modes of EMs are performed at UV or IR range and occurs in a time scale 100 fs. The EMs can be excited to higher states under UV laser illumination and this leads to decomposition [19,20]. Consequently, the ground electronic, vibrational states of EMs have been recognized to be prominent in the energy transferring processes.

Nitro-substituted arene compounds are very important in defence and civilian applications due to their interesting energetic properties [21]. However, the well-known polynitro arenes such as TNT, TATB, Picric acid etc. exhibit moderate performance [22]. Recently, it was reported that the derivatives of azole substituted polynitro-arenes enhance densities and performance [23]. Especially, the substitution of azoles i.e. triazole/tetrazole improves the positive heat of formation due to the higher amounts of nitrogen [24–27]. Kommu et al. reported that the tetrazole substituted polynitro-arene derivatives exhibit superior energetic properties those prevail over TNT [28]. In this regard, coherent anti-Stokes Raman spectroscopy (CARS) is an efficient technique to probe the ground state vibrational dynamics of the molecules with higher temporal and spectral resolutions in both gas and liquid phases [29–34]. CARS is a coherent, nonlinear technique in which all the inelastic Raman scattered photons emerge out in one direction as a laser. Employment of ultrafast lasers enables the novel possibilities of time and frequency-resolved CARS spectroscopies to probe the vibrational dynamics that occur in the time scales shorter than molecular vibration period ~100 fs. In a femtosecond time-resolved CARS (TR-CARS) experiment, several vibrational modes of the molecules can be excited simultaneously, and the relaxation processes can be probed in real-time. TR-CARS also enables us to estimate the dephasing times and collisional relaxation times of the interested vibrational modes in solutions. Additionally, TR-CARS investigate the excited state dynamics of vibrational modes. However, the excitation of molecular vibrational modes with fs broadband pulses in CARS experiment limits the spectral resolution, and it can be eliminated by employing pulse shaping techniques [35,36] to trigger selective absorptions. The analysis of TR-CARS spectra provokes the insight on intermolecular interactions as well as the molecular structure. To understand the molecular dynamics of the complex and nitrogen-rich EMs (tetrazole-N-(hetero) aryl derivatives namely 2,6-dinitro-4-(1H-tetrazole-1-yl)aniline ($C_7H_5N_7O_4$) and 1-(3,4,5-trinitrophenyl)-1H-tetrazole($C_7H_3N_7O_6$) femtosecond TR-CARS has been employed. To avoid the ambiguity in the description of the recorded TR CARS data, of two nitro substituted molecules, 2,6-dinitro-4-(1H-tetrazole-1-yl)aniline ($C_7H_5N_7O_4$) and 1-(3,4,5-trinitrophenyl)-1H-tetrazole($C_7H_3N_7O_6$) are labelled as 6 and 8, respectively.

2. Experiments

The experimental setup for TR-CARS is illustrated in Fig. 1. A Ti:-Sapphire based laser amplifier (LIBRA M/s Coherent) that delivers ultrafast pulses of central maximum 800 nm, pulse duration ~50 fs at 1 kHz repetition rate has been utilized in this experiment. The output of the amplifier at 800 nm is divided into two parts in a power ratio of 20:80using a plate beam splitter (BS1). One of the divided beams is employed as a pump to an optical parametric amplifier (OPA, TOPAS), which generates a wide range of tunable wavelengths to produce Stokes pulse of our interest. The other part of the beam from the beam splitter (20:80) is further divided into two equal parts, with the help of a 50:50 beam splitter (BS2), amongst one part play the role of the pump and the remaining part is the probe. The probe pulse is delayed with respect to the pump, stokes pulses and these delays are controlled by a Newport translation stage interfaced with ESP300 Universal motion controller. The three beams (Pump, Stokes and Probe) are arranged in a three-dimensional crossed beam phase matching (forward BOXCAR) configuration. The average energies of the pump, probe pulses and the Stokes pulse from OPA are measured to be ~0.6 μJ. These three pulses are focused by a planoconvex lens of focal length ~25 cm onto a quartz cuvette (of path length ~5 mm) that consisted the solution of tetrazole-N-(hetero) aryl derivatives dissolved in acetonitrile (sample 6 or sample 8). Usage of a lens with longer focal length in the experiment enhances the interaction volume, and it eventually leads to a significant CARS signal generation. The wavelengths of pump (ω_p) and probe (ω_{pr}) pulses were at 800 nm, whereas that of Stokes pulse from OPA was chosen to be 872 nm. Initially, the sample medium is pumped by the combination of both pump and Stokes pulses; later on, the delayed probe pulse interrogates the excited sample medium. Further, the pump and Stokes create the intramolecular coherence between the vibrational ground state and excited state that belongs to an electronic ground state. A delayed probe pulse scatters from the transient grating formed by the excited sample medium as the CARS signal (ω_{CARS}) when the required phase-matching condition is fulfilled. TR-CARS signals from the sample at different delay times of probe pulse are spatially filtered and allowed to enter into a spectrometer (MAYA 2000, M/s Ocean Optics). The samples 6 and 8 are dissolved in acetonitrile to prepare solutions with concentration of ~1 mM and were taken in a 5-mm quartz cuvette and placed in the focal plane, as shown in Fig. 1.

3. Results and discussion

The spontaneous Raman spectra (Horiba LabRAM HR –Evolution, at 785 nm exciting line) of samples 6 and 8 are illustrated in Fig. 2 and the corresponding Raman modes with their labels are summarized in Table 1. The theoretical calculations were performed with Gaussian software using functional B3LYP6-331G(DP) for the peak assignments. It is found that the experimental and calculated results were in good agreement.

3.1. Time-Resolved CARS

Fig. 3(a) and (b) show the time and frequency-resolved CARS spectra of sample 6 and 8, respectively, illustrated as contour maps at each probe delay, varying from −300 fs to 800 fs within a frequency range of 750–1850 cm^{-1}. The 2D contour plots showcase the complex nature of CARS signal with spectral features in the frequency domain and oscillation features in the time domain. These were confirmed by the vibrational modes in the frequency domain and Fourier transform of the transient CARS traces compound 6 and compound 8. The frequency-resolved CARS spectra at 200 fs, as illustrated in Fig. 3(c) and 3(d), are evidently free from the non-resonant background as around the zero delay. The loss of spectral resolution due to fs pulse probing is evident from Fig. 3(c) and (d) since several vibrational modes are simultaneously excited and overlapped on each other. Fig. 3(e) and (f) depict the CARS signal along with the pump and Stokes spectra, which confirm the blue-shifted CARS signal. Figs. 4 and 5 illustrate the time-resolved CARS (TR-CARS) signals for sample 6 modes investigated at 818 cm^{-1}, 1337 cm^{-1}, 1466 cm^{-1} and for the sample 8 modes studied at 841 cm^{-1}, 992 cm^{-1}, 1393 cm^{-1}, 1461 cm^{-1}, respectively. The TR-CARS signals have different features such as the non-resonant electronic background around zero delay, exponential decay arising from the population relaxation, and the oscillation which corresponds to the vibrational coupling. The TR-CARS trace has been fitted with a single exponential function that yields the average coherent vibrational decay time ~120–200 fs. Negative exponential fitting was carried out (Fig. 4 and Fig. 5) and error bars in the traces represent 5% error in the data, which can be attributed to the pulse to pulse energy fluctuations caused by the laser amplifier (a repetition rate of 1 kHz was used). The Fourier transform of the resonant TR-CARS trace reveals the vibrational couplings between different vibrational modes with quantum beat frequencies listed in Table 2. Due to the intramolecular vibrational mode interferences, quantum beats can be

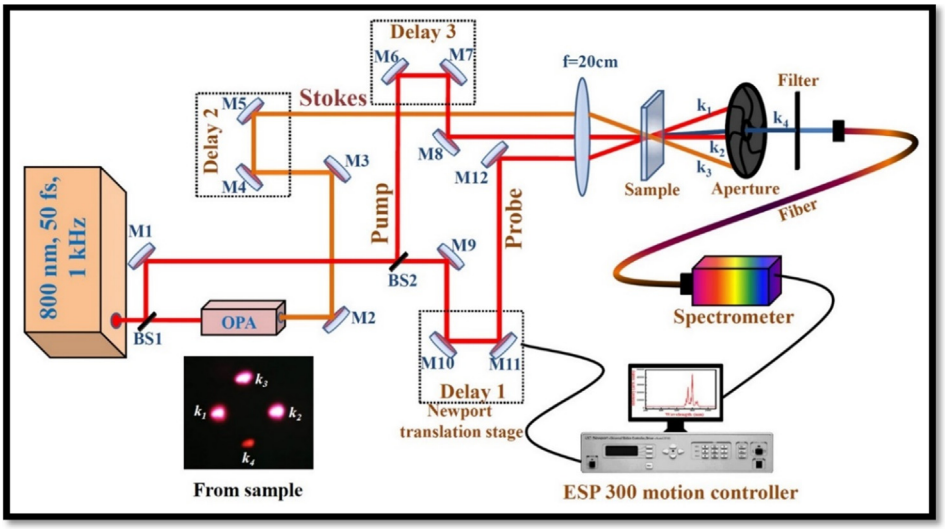

Fig. 1. Experimental set up of femtosecond TR-CARS. Inset depicts the CARS signal recorded in BOXCARS geometry for sample 6.

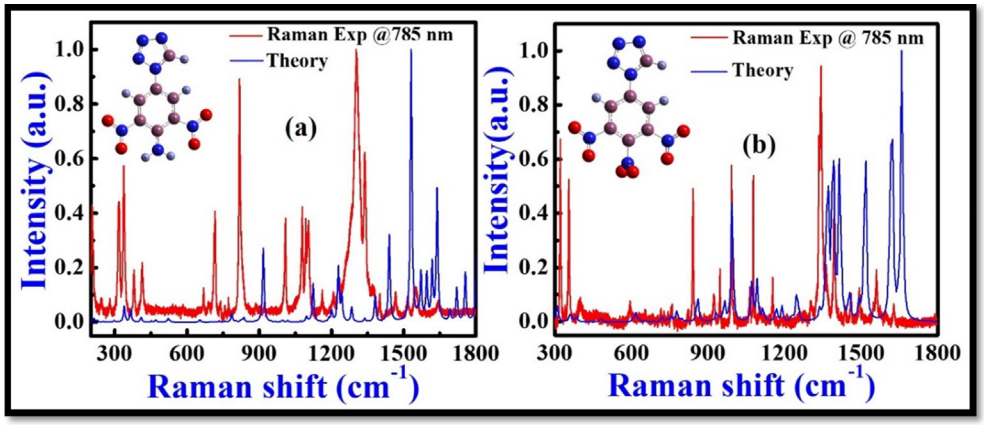

Fig. 2. Experimental and theoretical Spontaneous Raman spectra of compounds (a) 6 and (b) 8.

Table 1
Experimental and theoretical Raman modes and their labels for compound 6 and 8.

Experiment compound 6	Theory	Labelling	Experiment compound 8	Theory	Labelling
(υ_1) 720	711	H−N−H twisting	**(υ_1) 821**	796	C−H rocking, C═C═C wagging
(υ_2) 773	786	Ring elongation (Benzene)	**(υ_2) 841**	854	C−H wagging
(υ_3) 818	822	Ring deformation, NO_2 scissoring, N═N−N wagging	**(υ_3) 920**	914	C−H wagging
(υ_4) 920	916	Ring elongation, NO_2 scissoring, C═N stretching	**(υ_4) 946**	941	C−H wagging
(υ_5) 1006	1007	C−H wagging (tetrazole ring)	**(υ_5) 992**	994	N═N−N stretching (Tetrazole ring)
(υ_6) 1076	1071	C−H wagging (Benzene ring)	**(υ_6) 1077**	1073	C═H stretching, C−N stretching, N═N−N stretching, C−H rocking
(υ_7) 1109	1104	C−H wagging (Benzene ring)	**(υ_7) 1154**	1166	C−H rocking, ring elongation (Benzene ring)
(υ_8) 1207	1201	C−H rocking (Tetrazole and Benzene rings)	**(υ_8) 1302**	1338	N═N stretching, C═C═C asymmetric stretch
(υ_9) 1231	1228	C−N stretching, C-H rocking (Tetrazole and Benzene rings)	**(υ_9) 1335**	1338	N═N stretching, C═C═C asymmetric stretch
(υ_{10}) 1337	1338	N−N stretching, C−H wagging	**(υ_{10}) 1363**	1363	N═N stretching, C═C═C asymmetric stretch
(υ_{11}) 1374	1381	N−N stretching, C−H wagging	**(υ_{11}) 1460**	1453	C−H rocking, C═C stretching, C═N stretching
(υ_{12}) 1401	1389	H−N−H rocking, N═O stretching, C−H wagging	**(υ_{12}) 1493**	1492	C═N stretching, C═C stretching
(υ_{13}) 1466	1440	C═N stretching, ring stretching (Benzene), C−H rocking	**(υ_{13}) 1630**	1632	NO_2 asymmetric stretching, C═C═C asymmetric stretching (Benzene ring deformation)
(υ_{14}) 1517	1531	H−N−H scissoring, C═N stretching, C═C═C symmetric stretching, N═N stretching	**(υ_{14}) 1574**	1612	O═N═O asymmetric stretching, C═C═C asymmetric stretching
(υ_{15}) 1551	1558	C═C asymmetric stretching, NH_2 wagging, C−H wagging, N═O stretching	**(υ_{15}) 1628**	1632	O═N═O asymmetric stretching, C═C═C asymmetric stretching

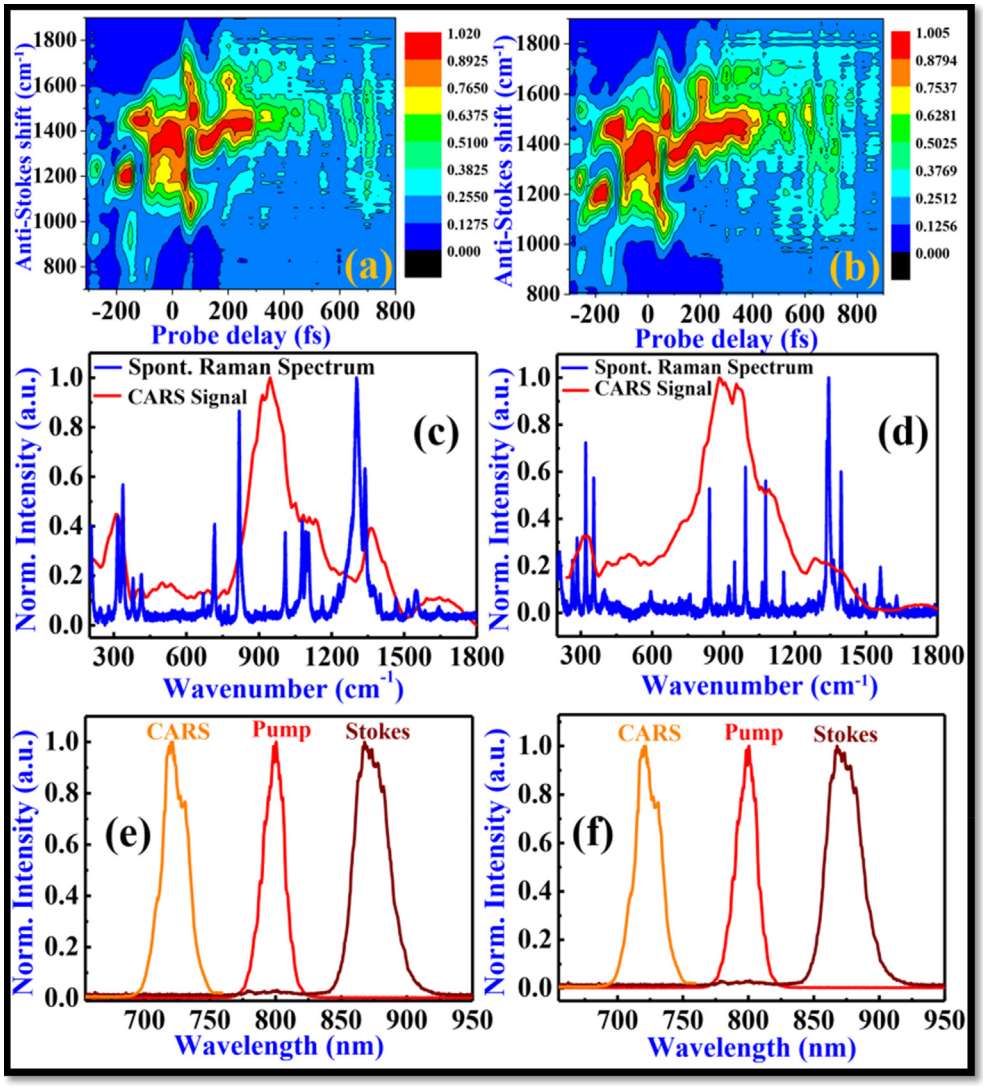

Fig. 3. Time-resolved CARS signal of compound (a) 6 and (b) 8 illustrating quantum beat structure. Spontaneous Raman (blue) and CARS signal (red) of (c) 6 and (d) 8 (e,f) Spectral profiles of the CARS signal, pump, and Stokes beams for the compounds 6 and 8, respectively.

obtained due to the coherent evolution of the quantum wave functions of the single molecule. Unlike vibrational polarization beats which are due to intermolecular vibrational mode interferences, quantum beats are the consequence of intra molecular vibrational mode interferences. The occurrence of vibrational polarization beats or quantum beats certainly depend on how the molecular medium has been probed. If the probe pulses energy density is above the dissociation threshold energy of the molecule under consideration, then vibrational polarization beats can be seen with shorter life times. With probe pulse energies below the threshold, CARS polarization is long-lived and, consequently, the contribution from different vibrational states will be cancelled out, due to which vibrational polarization beats may not be seen in the spectrum. Though we believe the observed oscillations are quantum beats, in principle one cannot ignore the occurrence of vibrational polarization beats those fall under the coherent excitation of the other molecules. Additionally, we cannot deny the possibility of the oscillations those arises due to the interference of molecular vibrational modes with the solvent modes of vibration [37].

In the present study, pump and stokes wavelengths utilized were ~800 nm, ~872 nm, respectively. The corresponding wavenumber difference is 1033 cm^{-1}. When tetrazole-N-(hetero)aryl derivatives dissolved in acetonitrile (ACN) are simultaneously excited by two pulses, the selective vibrational modes in the proximity of 1033 cm^{-1} are expected to be excited (parent modes). But it is evident from the data presented in Fig. 3(c) and Fig. 3(b) the other modes [daughter modes] far away from the direct excitation region (1033 cm^{-1}) were observed. This is possible only when there is an intramolecular vibrational coupling and hence the possibility of the intramolecular vibrational energy re-distribution among parent and daughter modes. The coherent excitation of the targeted mode relaxes through the IVR process because of the coupling of the neighbouring vibrational modes of a molecule. Based on the above-mentioned arguments, we could possibly argue the occurrence of IVR in the present time resolved CARS studies of tetrazoles (sample 6 and 8). The intramolecular vibrational relaxation (IVR) and their pathways of relaxations can be understood from the vibrational couplings since they arise from the coupling of vibrational modes of tetrazole derivatives. From Table 2, the vibrational couplings between several modes participating in the IVR process can be visualized as coupling of one mode with two or more vibrational modes. For instance, in sample 6, the modes υ_7, υ_8, and υ_{14}, and sample 8, υ_1, υ_3, υ_4, υ_7, and υ_{12} modes which are corresponding to the benzene ring and the tetrazole ring of the molecules, these vibrational modes might participate (energy transfer process in IVR) [38,39]. The vibrational modes which are interacting with only one vibrational mode such as υ_1 to υ_6, υ_9 to υ_{13}, υ_{15}, υ_{16} in 6 and υ_2, υ_5, υ_6, υ_8 to υ_{11}, υ_{13} to υ_{15} in 8 are corresponding to the C—N, C═C, C—H and NO_2 stretching vibrational

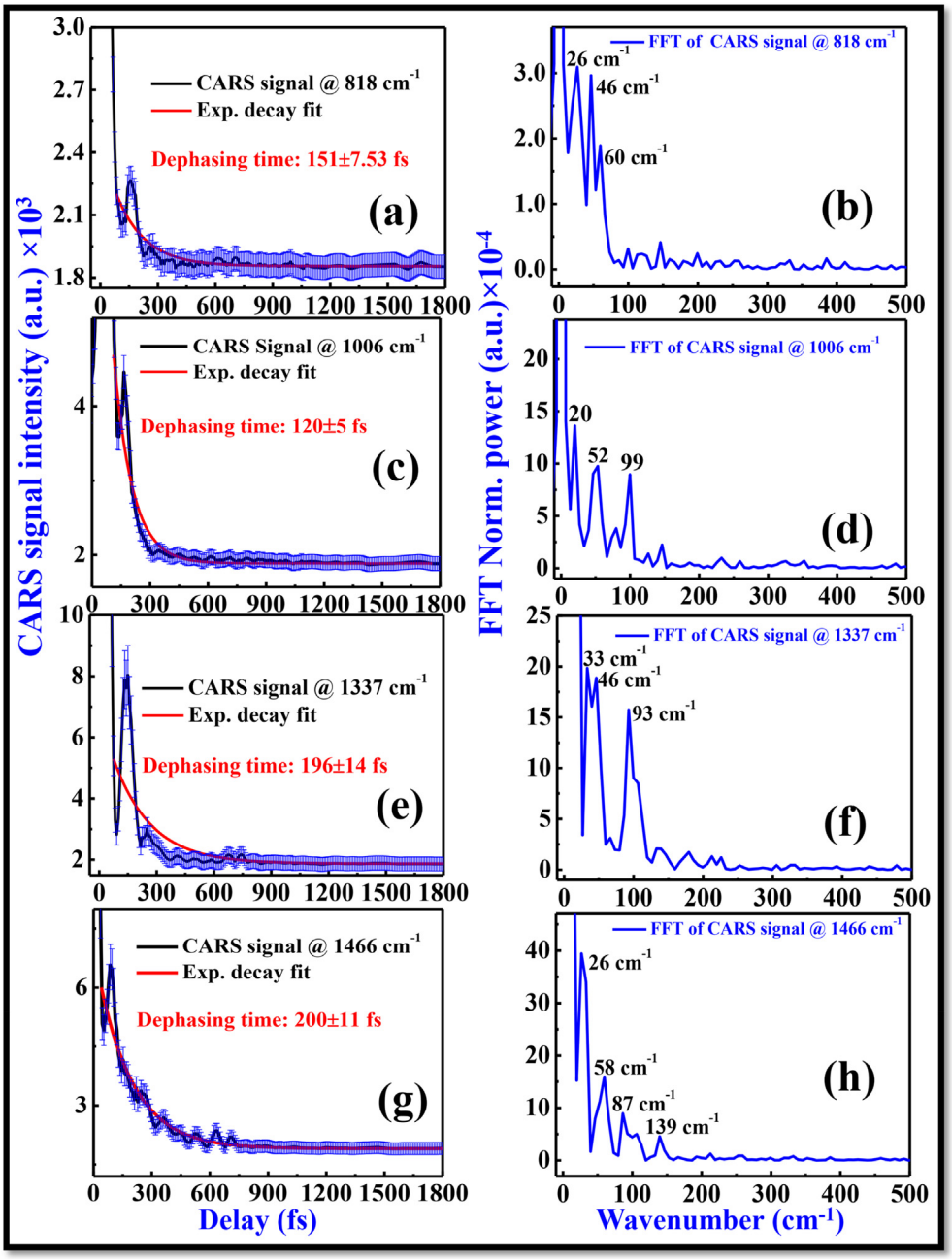

Fig. 4. (a, c, e, f) TR-CARS signal and their corresponding fast Fourier transforms (b, d, f, h) for the 818 cm^{-1}, 1006 cm^{-1}, 1337 cm^{-1} and 1466 cm^{-1} modes from sample 6. Negative exponential fitting was carried out and error bars were kept in the traces to represent 5% error in the data points which can be attributed to the pulse to pulse energy fluctuations caused by the laser amplifier (1 kHz repetition rate).

modes of tetrazole and benzene rings and these modes could be involved in the initial decomposition process. The vibrational modes which are very active in interacting with other vibrational modes have a significant tendency to transfer energy through IVR. Yu et al. [40] reported on the intramolecular vibrational redistribution in RDX molecules using multiplex CARS technique. According to them, the low-frequency vibrational modes such as phonon modes are the doorways of energy transfer from outside to the inside of RDX molecule. Further, the vibrational modes which are mostly involved in IVR are found to carry the vibrational energy to the higher frequency states in IVR. In the multi-phonon up-pumping the low frequency vibrational modes which match to the frequency of phonons are the energy portals from outside to inside of the molecules. Comparison of the exponential decay trends of TR-CARS traces demonstrates that the sample 8 exhibit a faster decay than sample 6. The reason could be the presence of an extra NO_2 group in sample 8, attempting a faster IVR.

From Figs. 4, 5 data it is evident that the low energy modes those corresponding to the C-H vibrations exhibited faster average dephasing times compared to higher energy vibrational modes. Consequently, the C-H vibrational modes could be excited first upon photoexcitation and causing an initial chemical reaction. Since we are not using extremely short laser pulses (shorter than 10 fs), selective excitation may be possible with the laser pulses utilized in the present experiment. Consequently, we believe that the probe pulses (~70 fs) might provide a significant spectral resolution and, hence, the measured decay time scales are approximated to a significant accuracy. However, with time and frequency resolved CARS these effects can be minimized [41]. Several vibrational modes will participate in the IVR processes mainly

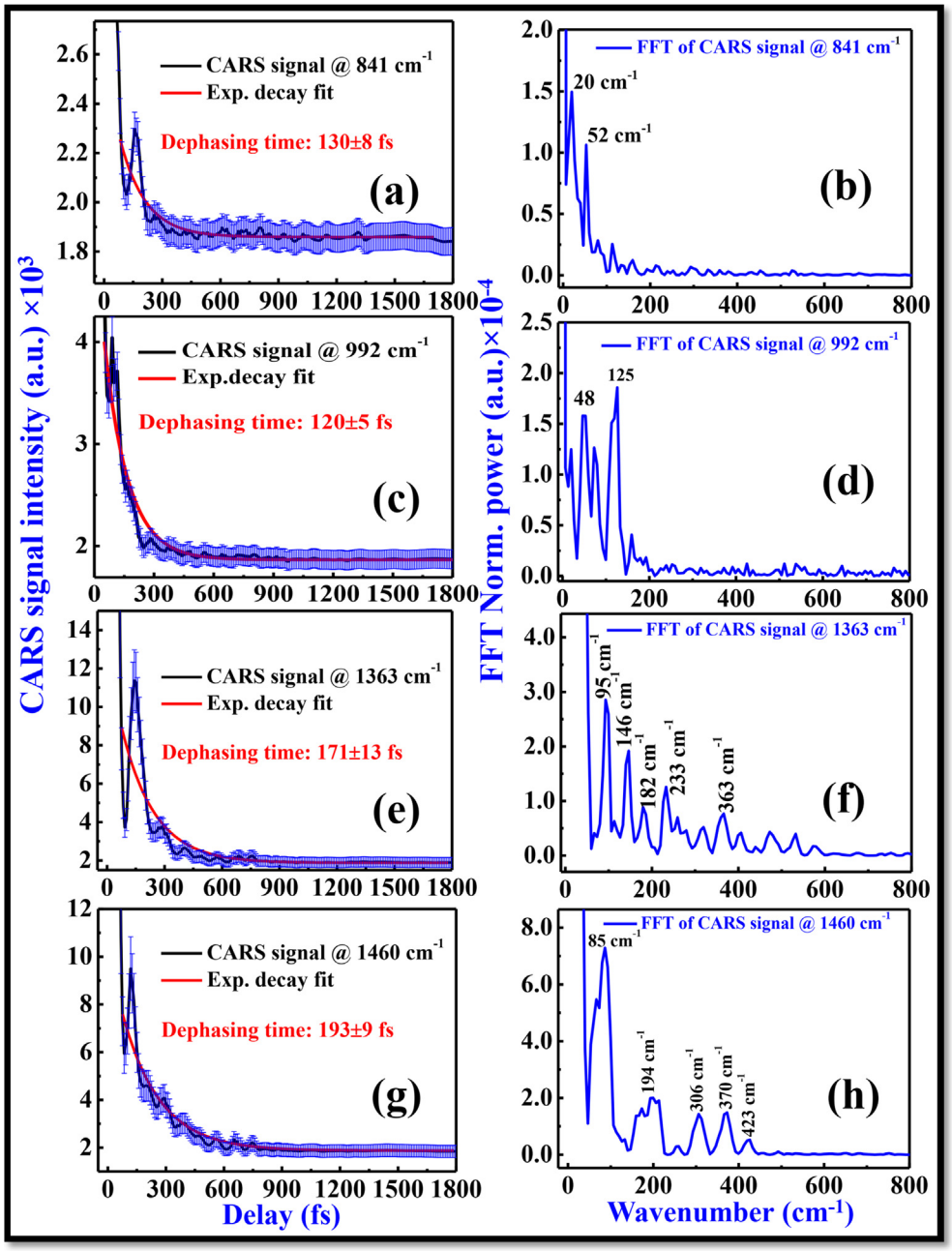

Fig. 5. (a, c, e, g) TR-CARS signal and their corresponding fast Fourier transforms (b, d, f, h) at 841 cm^{-1}, 992 cm^{-1}, 1363 cm^{-1} and 1460 cm^{-1} from sample 8. Negative exponential fitting was carried out and error bars were kept in the traces to represent 5% error in the data points which can be attributed to the pulse to pulse energy fluctuations caused by the laser amplifier of rep rate 1 kHz.

in polyatomic molecules (explosives) in order to track IVR high temporal resolution, broadband excitation capability and coherent detection capability are a prerequisite. It was evident from the literature that the Raman modes of ACN are 380 cm^{-1}, 918 cm^{-1}, 1376 cm^{-1}, 1440 cm^{-1}, 2249 cm^{-1}, 2942 cm^{-1}. Additionally, we did not observe any solvent effects in these measurements. We recorded the CARS trace of pure acetonitrile (ACN) alone and could not see any Raman signatures of ACN vibrational modes. The recorded data of the solvent is shown in Fig. 6(a). Moreover, the pump (800 nm), Stokes (872 nm) beam wavelengths both were far from the absorption maximum 320–380 nm of the ACN solvent. We do believe that the selected pump wavelengths are not in resonance with ACN absorption and perhaps this resulted in no Raman signatures for the pure solvent. Further, the intensity dependent CARS signal with a slope of 2.1 ensures the presence of third-order NLO (CARS) process as shown in data of Fig. 6(b).

Additionally, the relationship between IVR and solvent assisted vibrational energy transfer (VET) is extremely complex to understand even for simple molecules too. The molecules in the present study are novel tetrazoles require an extensive study to claim on relationship between IVR and solvent (ACN) assisted VET both qualitatively and quantitatively. Though the theoretical/experimental vibrational mode frequencies of tetrazoles are known, to comment on solvent assisted vibrational energy redistribution (IVR), instantaneous normal mode solvent spectrum that can be derived from force-force auto correlation functions is required. [42] Further, earlier reports suggest that [43,44] the solvent assisted IVR decays are longer in timescales and even be extended to few picoseconds. But the decay time scales obtained in the present experimental study are in the femtosecond domain, which confirms that there are no such significant solvent effects on IVR. Besides this, Hiromi et al. [45] mentioned that solute–solvent effects play

Table 2
Possible vibrational coupling between the vibrational modes of tetrazole derivatives.

Beat frequency (cm^{-1}) of 6	Contributing modes (cm^{-1})	Beat frequency (cm^{-1}) of 8	Contributing modes (cm^{-1})
26	(υ_1) 715 and 740 (υ_2)	20	(υ_1) 821 and 840 (υ_2)
46	(υ_3) 773 and 820 (υ_4)	52	(υ_1) 821 and 870 (υ_3)
60	(υ_5) 758 and 820 (υ_4)	48	(υ_1) 821 and 870 (υ_3)
20	(υ_6) 1079 and 1103 (υ_7)	125	(υ_3) 870 and 992 (υ_4)
52	(υ_7)1103 and 1161(υ_8)	95	(υ_7) 1302 and 1394 (υ_{11})
99	(υ_7) 1103 and 1208 (υ_9)	146	(υ_9) 1342 and 1493 (υ_{12})
33	(υ_{10}) 1303 and 1338 (υ_{11})	182	(υ_6) 1153 and 1335 (υ_8)
46	(υ_8) 1161 and 1208 (υ_9)	233	(υ_8) 1335 and 1574 (υ_{14})
93	(υ_{12}) 1374 and 1466 (υ_{14})	363	(υ_4) 992 and 1363 (υ_{10})
26	(υ_{12}) 1374 and 1401 (υ_{13})	85	(υ_{13}) 1549 and 1628 (υ_{15})
58	(υ_{14}) 1466 and 1517 (υ_{15})	194	(υ_7) 1302 and 1493 (υ_{12})
87	(υ_{14}) 1466 and 1551 (υ_{16})	306	(υ_4) 992 and 1302 (υ_7)
139	(υ_8) 1161 and 1303 (υ_{10})	370	(υ_4) 992 and 1363 (υ_{10})
–	–	423	(υ_5) 1063 and 1493 (υ_{12})

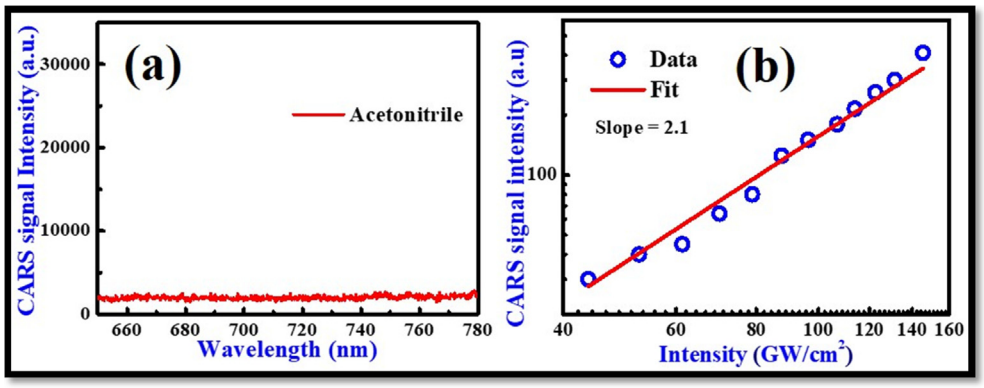

Fig. 6. (a) Spectra of pure acetonitrile solvent at zero-time delay (b) intensity dependent CARS signal.

a very little role in the process of IVR.

Though we describe the decay of quantum beats on the basis of intramolecular vibrational energy redistribution (IVR), the mentioned decay is complicated due to unidentified molecular dynamics of decoherence. In addition to the IVR, other possible decoherence processes include population decay, vibrational cooling (VC), occurring within the molecule until it thermalizes the obtained excitation energy to the surrounding liquid phonon bath through the cascade vibrational relaxation processes [46]. Other possibility of the decoherence of the modes might be from the damping of vibrations of a particular molecule due to the inelastic collision with the surrounding molecules [47]. Finally, we proclaim that the results (quantum beats and temporal measurements of the decays) produced in the manuscript are certainly reproducible with the same accuracy (within experimental errors). Moreover, as discussed by Nath et al. [41,48] recovery of Raman spectrum from time frequency domain in coherent Raman processes is less sensitive to experimental noises and fluctuations in pulse energies. Additionally, we could say the obtained beats from the FFT of the CARS trace beyond time zero are not experimental artifacts rather they are the Raman signatures of the solute. We could confirm this on the grounds of repeatability of the beats in different trails.

The beats were achieved by performing the FFT on the normalized CARS spectra. The corresponding FFT frequency was then converted to wavenumber by using following equation (1).

$$\nu(cm^{-1}) = \frac{FFT\,(frequency) * 10^5}{3} \tag{1}$$

Coherent vibrational decay time (T_2) relates with the line width of the Raman mode under consideration as shown in the equation (2)

$$\Delta\nu = \frac{1}{2\pi c T_2} \tag{2}$$

The Raman peak width corresponding to the 818 cm^{-1} was measured to be ~9.8 cm^{-1} whereas that from the measured average dephasing time (T_2) was ~35 cm^{-1}. This shows that, the decay must be longer than the estimated ~150 fs. However, we cannot completely and confidently explain the observed discrepancy. The fast decay of the coherent vibrational mode could possibly be understood in the following manner. In the present study, the measured decay is the average dephasing time (T_2) that comprises two contributions, namely the pure dephasing time (τ_{ph}) and life time of a vibrational excited state (T_1) of the as in the following equation (3)

$$\frac{1}{T_2} = \frac{1}{2T_1} + \frac{1}{\tau_{ph}} \tag{3}$$

(i) Recently, it was demonstrated that the fast/slow decay of a coherent vibration depends on whether the mode of interest is symmetric or asymmetric [56]. According to the experiments by Kozai et al. [49] coherent vibrational decay of an asymmetric mode is faster compared to a symmetric vibrational mode. Therefore, the symmetry of the mode 818 cm^{-1} in the present case, corresponding to ring deformation, NO_2 scissoring, N=N–N wagging, could have resulted in the fast-coherent vibrational decay ~150 fs (ii) Another possibility is the fast decay of the vibrational mode may quench of the pure dephasing mechanisms [29]. Keifer et al. [33] also observed similar fast average dephasing times (~350 fs) in the case of Imidazolium ionic liquids. As these tetrazole compounds are novel and this kind of work in these molecules is not yet attempted by any group, we could only explain the vibrational dynamics of tetrazole compounds limitedly.

4. Conclusions

In summary, fs TR-CARS experiments have been performed to study the intramolecular vibrational dynamics of the nitro substituted tetrazole-N-(hetero)aryl derivatives in solution. Excitation and relaxation of selected modes of two new molecules (6 and 8) were studied. The average dephasing time was observed to occur in a time scale ~120–200 fs and demonstrate that the intramolecular vibrational energy redistribution occurs in the same time scale. FFT of the TR-CARS traces revealed beat frequencies, which might correspond to the modes those involved in the inherent vibrational coupling of IVR. The results provided in this study offer an intuition of the ultrafast response of these molecules and a basic insight of photon-induced chemistry of these novel EMs.

CRediT authorship contribution statement

Naga Krishnakanth Katturi: Conceptualization, Methodology, Investigation, Formal analysis, Validation, Writing - original draft. **Sarang Dev G:** Investigation, Formal analysis. **Nagarjuna Kommu:** Investigation, Formal analysis. **Gopala Krishna Podagatlapalli:** Conceptualization, Methodology, Investigation, Formal analysis, Validation, Writing - original draft. **Venugopal Rao Soma:** Conceptualization, Resources, Writing - original draft, Supervision, Project administration, Funding acquisition.

Declaration of Competing Interest

The authors declare that they have no known competing financial interests or personal relationships that could have appeared to influence the work reported in this paper.

Acknowledgements

We thank the DRDO, India, for financial support through the project #ERIP/ER/1501138/M/01/319/D(R&D). We also thank Mr. G. Damarla for help in Gaussian simulations.

Appendix A. Supplementary material

Supplementary data to this article can be found online at https://doi.org/10.1016/j.cplett.2020.137843.

References

[1] M. Schmitt, G. Knopp, A. Materny, W. Kiefer, J. Phys. Chem. A 102 (23) (1998) 4059–4065.
[2] M. Schmitt, T. Siebert, A. Grabtchikov, V. Orlovich, W. Kiefer, Asian J. Phys. 12 (1) (2003) 1.
[3] M. Heid, S. Schlücker, U. Schmitt, T. Chen, R. Schweitzer-Stenner, V. Engel, W. Kiefer, J. Raman Spectrosc. 32 (9) (2001) 771–784.
[4] M. Heid, T. Chen, U. Schmitt, W. Kiefer, Chem. Phys. Lett. 334 (1–3) (2001) 119–126.
[5] J. Sharma, B.C. Beard, M. Chaykovsky, J. Phys. Chem. 95 (3) (1991) 1209–1213.
[6] M.M. Kuklja, B.P. Aduev, E.D. Aluker, V.I. Krasheninin, A.G. Krechetov, A.Y. Mitrofanov, J. Appl. Phys. 89 (7) (2001) 4156–4166.
[7] A. Bhattacharya, Y. Guo, E.R. Bernstein, Acc. Chem. Res. 43 (12) (2010) 1476–1485.
[8] G. Chu, F. Lu, J. Xin, T. Xi, M. Shui, W. He, Y. Gu, Y. Xiong, K. Cheng, T. Xu, RSC Adv. 6 (60) (2016) 55560–55567.
[9] Z.A. Dreger, Y.A. Gruzdkov, Y.M. Gupta, J.J. Dick, J. Phys. Chem. B 106 (2) (2002) 247–256.
[10] E.A. Zhurova, V.G. Tsirelson, A.I. Stash, M.V. Yakovlev, A.A. Pinkerton, J. Phys. Chem. B 108 (52) (2004) 20173–20179.
[11] W. Zhu, H. Huang, H. Huang, H. Xiao, J. Chem. Phys. 136 (4) (2012) 044516.
[12] N.-N. Ge, Y.-K. Wei, G.-F. Ji, X.-R. Chen, F. Zhao, D.-Q. Wei, J. Phys. Chem. B 116 (46) (2012) 13696–13704.
[13] R. Thurston, M.M. Brister, L.Z. Tan, E.G. Champenois, S. Bakhti, P. Muddukrishna, T. Weber, A. Belkacem, D.S. Slaughter, N. Shivaram, J. Phys. Chem. A (2020).
[14] M.-W. Chen, S. You, K.S. Suslick, D.D. Dlott, Appl. Phys. Lett. 104 (6) (2014) 061907.
[15] Y. Sun, M. Shui, T. Xu, Y. Shu, X. Wang, Z. Zhao, Y. Gu, Asian J. Chem. 25 (8) (2013) 4247–4250.
[16] D.D. Dlott, M.D. Fayer, J. Chem. Phys. 92 (6) (1990) 3798–3812.
[17] S. Chen, W.A. Tolbert, D.D. Dlott, J. Phys. Chem. 98 (32) (1994) 7759–7766.
[18] D.J. Nesbitt, R.W. Field, J. Phys. Chem. 100 (31) (1996) 12735–12756.
[19] C. Rajchenbach, G. Jonusauskas, C. Rulliere, Le Journal de Physique IV 05(C4) (1995) C4-365-C4-378.
[20] V.M. Kenkre, A. Tokmakoff, M.D. Fayer, J. Chem. Phys. 101 (12) (1994) 10618–10629.
[21] K. Menke, Organic Chemistry of Explosives, J. P. Agrawal, R. D. Hodgson, Propellants, Explosives, Pyrotechnics 32(2) (2007) 182-182.
[22] Z. Zeng, Y. Guo, B. Twamley, J.M. Shreeve, Chem. Commun. 40 (2009) 6014.
[23] H. Gao, J.n.M. Shreeve, Chemical Reviews 111(11) (2011) 7377-7436.
[24] N. Kommu, V.D. Ghule, A.S. Kumar, A.K. Sahoo, Chem. Asian J. 9 (1) (2013) 166–178.
[25] A.S. Kumar, N. Kommu, V.D. Ghule, A.K. Sahoo, J. Mater. Chem. A 2 (21) (2014) 7917.
[26] N. Kommu, A.S. Kumar, J. Raveendra, V.D. Ghule, A.K. Sahoo, Asian J. Org. Chem. 5 (1) (2015) 138–146.
[27] A.S. Kumar, V.D. Ghule, S. Subrahmanyam, A.K. Sahoo, Chem. - A European J. 19 (2) (2012) 509–518.
[28] N. Kommu, M. Balaraju, V.D. Ghule, A.K. Sahoo, J. Mater. Chem. A 5 (16) (2017) 7366–7371.
[29] M. Namboodiri, M.M. Kazemi, T. Zeb Khan, A. Materny, J. Kiefer, J. Am. Chem. Soc. 136 (16) (2014) 6136–6141.
[30] Y. Zhao, S. Zhang, B. Zhou, Z. Dong, D. Chen, Z. Zhang, Y. Xia, J. Raman Spectrosc. 45 (9) (2014) 826–829.
[31] K. Niu, S.-Y. Lee, J. Chem. Phys. 136 (6) (2012) 064504.
[32] P.J. Wrzesinski, H.U. Stauffer, W.D. Kulatilaka, J.R. Gord, S. Roy, J. Raman Spectrosc. 44 (10) (2013) 1344–1348.
[33] J. Kiefer, M. Namboodiri, M.M. Kazemi, A. Materny, J. Raman Spectrosc. 46 (8) (2015) 722–726.
[34] S.R. Engel, J.D. Miller, C.E. Dedic, T. Seeger, A. Leipertz, T.R. Meyer, J. Raman Spectrosc. 44 (10) (2013) 1336–1343.
[35] J.M. Levitt, O. Katz, Y. Silberberg, J. Mod. Opt. 61 (10) (2014) 872–876.
[36] P.V. Kolesnichenko, J.O. Tollerud, J.A. Davis, APL Photonics 4 (5) (2019) 056102.
[37] J. Faeder, I. Pinkas, G. Knopp, Y. Prior, D. Tannor, J. Chem. Phys. 115 (18) (2001) 8440–8454.
[38] Y. Guo, M. Greenfield, E. Bernstein, J. Chem. Phys. 122 (24) (2005) 244310.
[39] J.E. Patterson, Z.A. Dreger, M. Miao, Y.M. Gupta, J. Phys. Chem. A 112 (32) (2008) 7374–7382.
[40] G. Yu, Y. Zeng, W. Guo, H. Wu, G. Zhu, Z. Zheng, X. Zheng, Y. Song, Y. Yang, J. Phys. Chem. A 121 (13) (2017) 2565–2571.
[41] S. Nath, D.C. Urbanek, S.J. Kern, M.A. Berg, Phys. Rev. Lett. 97 (26) (2006) 267401.
[42] V. May, O. Kühn, Charge and energy transfer dynamics in molecular systems, John Wiley & Sons, 2008.
[43] J. Assmann, R.V. Benten, A. Charvat, B. Abel, J. Phys. Chem. A 107 (12) (2003) 1904–1913.
[44] J.C. Deàk, L.K. Iwaki, S.T. Rhea, D.D. Dlott, J. Raman Spectrosc. 31 (4) (2000) 263–274.
[45] H. Okamoto, K. Yoshihara, Chem. Phys. Lett. 177 (6) (1991) 568–572.
[46] S. Shigeto, Y. Pang, Y. Fang, D.D. Dlott, J. Phys. Chem. B 112 (2) (2008) 232–241.
[47] W.-Y. Wang, N. Sui, L.-Q. Zhang, Y.-H. Wang, L. Wang, Q. Wang, J. Wang, Z.-H. Kang, Y.-Q. Yang, Q. Zhou, Chin. Phys. B 27 (10) (2018) 104205.
[48] S. Nath, D.C. Urbanek, S.J. Kern, M.A. Berg, J. Chem. Phys. 127 (4) (2007) 044307.
[49] T. Kozai, Y. Kayano, T. Aoi, N. Tsurumachi, S. Nakanishi, J. Raman Spectrosc. 46 (4) (2015) 384–387.